

pubs.acs.org/cm Article

Harnessing the Materials Chemistry of Mesoporous Silicon Nanoparticles to Prepare "Armor-Clad" Enzymes

Yi-Sheng Lu, Ruhan Fan, Willem Vugs, Lieuwe Biewenga, Ziming Zhou, Sanahan Vijayakumar, Maarten Merkx, and Michael J. Sailor*



Cite This: Chem. Mater. 2023, 35, 10247-10257



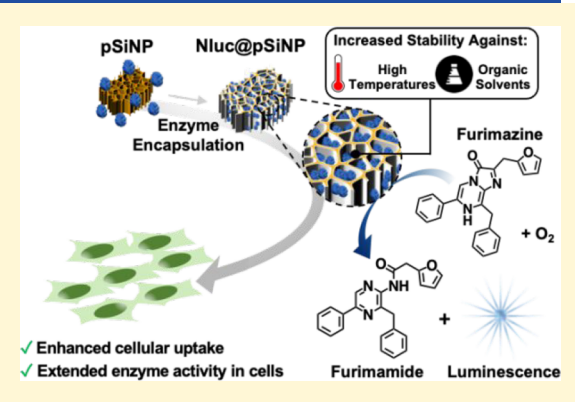
ACCESS I

III Metrics & More

Article Recommendations

SI Supporting Information

ABSTRACT: There is a growing interest in nanomaterials that can encapsulate enzymes while retaining their ability to function within the confines of a nanocage. Here porous silicon nanoparticles (pSiNPs) are evaluated as an enzyme cage, utilizing the aqueous chemistry of silicon to dynamically restructure the mesopore structure, immobilizing, and confining the enzyme. The common bioluminescent reporter enzyme nanoluciferase (Nluc) is used to evaluate two different trapping chemistries, and impacts on the stability and catalytic performance of the enzyme are compared with controls involving free enzyme and enzyme electrostatically adsorbed to a pSiNP host without the use of trapping chemistry. The two chemistries exploited in this study are (1) oxidative trapping, where mild aqueous oxidation of the elemental silicon skeleton in the mesoporous silicon host swells and restructures the pore walls, physically trapping the Nluc payload



in a porous SiO_2 matrix, and (2) calcium ion-induced condensation, where localized precipitation of calcium silicate entraps the Nluc protein in a porous silicate matrix. The two trapping chemistries form robust nanoscale cages with substantially smaller pores (9.8 \pm 0.4 and 8.8 \pm 0.3 nm, respectively) compared to the pSiNP starting material (15.3 \pm 1.8 nm), such that the enzyme does not leach from the pSiNPs in aqueous buffer or under assay conditions. Enzyme stability is substantially improved using the two trapping chemistries; the caged materials retain 30–45% activity after heating to 80 °C for 30 min or when exposed to organic solvents; either of these denaturing conditions result in complete or near-complete loss of activity for the free enzyme or for enzyme that is electrostatically adsorbed to pSiNPs. Finally, we explore the potential for the use of the Nluc-encapsulated nanocomposite as a cellular probe by demonstrating the luminescent reporting function of the nanoparticles in HeLa human cell cultures.

■ INTRODUCTION

Whereas free enzymes are often used in industrial-based applications and manufacturing processes, the natural environment for such biologic catalysts generally involves some type of physical confinement, either in a membrane or in a subcellular compartment. These hosts serve to stabilize the proteins and optimize their function. Similarly, the incorporation of enzymes within nanomaterial-based hosts offers a strategy to improve performance, extend lifetime, and increase operating stability under conditions that would normally be detrimental to enzyme function.²⁻⁷ Here broader considerations in terms of processability, biocompatibility, leaching, and direct delivery of enzymes into a targeted location are of significant importance for applications in biomedical and other healthrelated fields.⁸⁻¹⁰ Extensive research effort has been expended on the development of enzyme host materials and immobilization strategies based on adsorption, covalent conjugation, pore infiltration and in situ synthesis (i.e., coprecipitation, biomineralization). 11-13 However, it remains a challenge to develop general approaches to prepare encapsulated enzymes that satisfy all of the above constraints.

Porous silicon nanoparticles (pSiNPs), a class of biodegradable nanomaterials with versatile properties, have emerged as an attractive host matrix for encapsulation of a wide range of biomolecules. Hecently, it has been shown that the mesopore structure of pSiNPs undergoes a restructuring process in aqueous solution that can constrict the pores and physically trap a biomolecule or other molecular payload. Underlying this dynamic nature is the ability of pSiNPs to accommodate enzymes with sizes spanning the low mesopore regime (2–15 nm) while simultaneously stabilizing them via pore confinement. Harnessing this process for encapsulation and preservation of enzyme activity is highly desirable, and it is enabled by the electrochemical process used to prepare pSi, which allows tuning of pore sizes with

Received: October 15, 2023 Revised: November 5, 2023 Accepted: November 6, 2023 Published: November 24, 2023





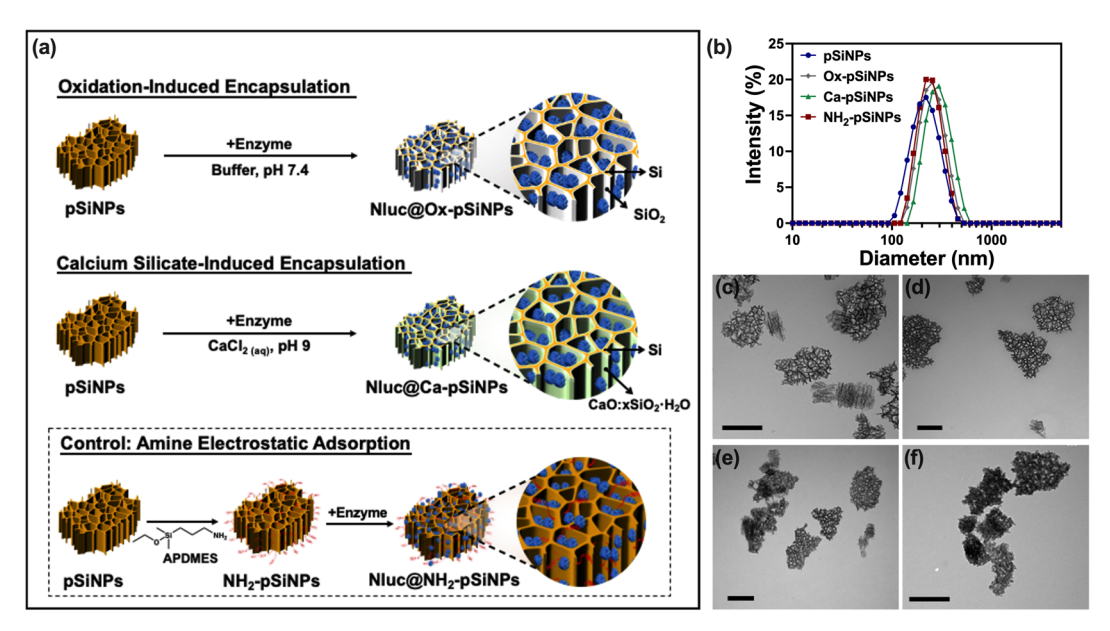


Figure 1. Design and characterization of enzyme encapsulation chemistries used on pSiNP hosts. (a) Schematic illustrating the two approaches used to trap the enzyme Nluc in pSiNPs: "Oxidation-Induced Encapsulation" (Ox-pSiNPs) involves mild oxidation of the silicon skeleton on the pSiNPs that physically traps the Nluc within the nanostructure; "Calcium Silicate-Induced Encapsulation" (Ca-pSiNPs) involves immobilization of Nluc via the formation of a calcium silicate precipitate within the porous matrix of the pSiNPs. The two trapping chemistries were compared to a control formulation, "Amine Electrostatic Adsorption" (NH₂-pSiNPs), prepared by first modifying the inner pore walls of the pSiNP with a primary amine, which then binds Nluc via electrostatic interactions. (b) Dynamic light scattering intensity distributions comparing the hydrodynamic size distribution of pSiNPs resulting from each encapsulation chemistry. (c-e) Transmission electron microscope (TEM) images of: (c) as-prepared pSiNPs; (d) NH₂-pSiNPs; (e) Ox-pSiNPs; and (f) Ca-pSiNPs. Scale bar in each image is 200 nm.

nanometer resolution—a feature that is not as readily achieved with other host materials. ^{2,4,5,21,22} The process employed in the present work can be considered to be analogous to *in situ* syntheses based on biosilicification, metal—organic frameworks (MOFs)^{12,22} or covalent—organic frameworks (COFs), whereby the host matrix is assembled around the enzyme molecules to overcome the limitations imposed by post-infiltration into a host matrix of a fixed pore size. While these materials have shown great utility, they can involve complex preparation conditions, can show compatibility issues with some proteins, and/or can exhibit toxicity associated with leaching of metal ions or framework ligands, which places limits on their use in biological or biomedical applications. ^{23,24}

Given their facile tunability and established biocompatibility, we reasoned that pSiNPs might act as a generalizable host matrix to prepare robust enzyme-inorganic nanocomposites suitable for biological applications. It is worth mentioning that much of the prior emphasis for pSiNPs has been as an enzyme delivery system from which the enzyme is released as a free molecule into solution, where its function is harnessed in its native state. 16,25 However, there are few studies involving the function of enzymes while immobilized in a porous silicon host, and the influence of pSiNP-relevant surface chemistry, immobilization chemistry, and other host-matrix effects on the activity and stability of an enzyme guest has not been explored in detail. 26-29 Two key issues here are (1) how to immobilize an enzyme into pSiNPs while retaining its activity and (2) whether the structural and chemical properties of pSiNPs can afford improved performance for envisioned catalytic applications.

To address the above questions, this study utilized immobilization strategies involving *in situ* aqueous oxidation and precipitation of calcium silicate within the pore walls of

pSiNPs to encapsulate a model enzyme, nanoluciferase (Nluc) (Figure 1a). We chose the enzyme Nluc as a payload due to its convenient chemiluminescent readout and its utility for a host of cellular assays.³⁰ The luminescence that is generated when Nluc catalyzes the oxidation of its substrate, the small molecule furimazine, 31 allowed a direct measurement of activity while also providing a means to visually discern if the catalyst was performing its function. Structural and analytical investigations showed that the oxidation- and calcium silicate-induced encapsulation chemistries (Nluc@Ox-pSiNPs and Nluc@CapSiNPs) both exhibit superior performance in minimizing enzyme leaching and in protecting the enzyme against thermalor organic-solvent-induced denaturation compared with control pSiNPs wherein the enzyme was electrostatically adsorbed to the amine-modified inner pore walls of the pSiNPs. Finally, a set of experiments were performed that evaluated the compatibility of the encapsulated construct Nluc@Ox-pSiNP with live cells and with common cellular assay reagents, which established the suitability of the caged enzymes as cellular probes.

■ RESULTS AND DISCUSSION

Preparation and Characterization of Nluc@pSiNP Constructs. The two trapping chemistries, Oxidation-Induced Encapsulation (Ox-pSiNPs) and Calcium Silicate-Induced Encapsulation (Ca-pSiNPs), along with the chemistry used to prepare the control formulation Amine Electrostatic Adsorption (NH₂-pSiNPs), are outlined in Figure 1a. The Oxidation-Induced Encapsulation method followed a previously published route involving treatment of pSiNPs with aqueous phosphate buffered saline (PBS) buffer (at pH 7.4) in the presence of the protein 32 to simultaneously induce mild oxidation of the pSiNP skeleton and trap Nluc within the

nanostructure. The Calcium Silicate-Induced Encapsulation approach followed the previously reported 19 ability of added Ca (II) ions to react with orthosilicate species created at the pSiNP surface during its dissolution at pH 9, to form a calcium silicate precipitate that entrapped dissolved Nluc within the pores. The Amine Electrostatic Adsorption chemistry was based on the ability of proteins to adsorb to an oppositely charged surface. In the present case, electrostatic adsorption of Nluc was effected at neutral pH, where the net anionic charge on the Nluc (pI = 5.7) was attracted to an amine-terminated, positively charged pSiNP surface. The amines had been previously grafted to the pSiNPs using 3-aminopropyldimethylethoxysilane (APDMES). Such electrostatic adsorption has been shown to yield a relatively weak association between the adsorbed protein and the surface that is readily disrupted in aqueous solutions containing ions. 19 In this work, empty particles with the Oxidation-Induced Encapsulation, Calcium Silicate-Induced Encapsulation, and Amine Electrostatic Adsorption immobilization chemistries are denoted as OxpSiNPs and Ca-pSiNPs, and NH2-pSiNPs, respectively, and the corresponding Nluc-loaded pSiNP formulations are referred to as Nluc@Ox-pSiNPs and Nluc@Ca-pSiNPs and Nluc@NH₂-pSiNPs, respectively.

The starting material pSiNP hosts were prepared following a previously reported "electrochemical perforation etch" procedure.33 This involved pulsed electrochemical anodization of single crystal silicon wafers to generate a stratified porous silicon layer, followed by removal of the porous layer, which was then subjected to ultrasonic fracture to yield the pSiNPs. The as-prepared pSiNPs (prior to enzyme encapsulation) exhibited a mean hydrodynamic diameter of 211 ± 6 nm and zeta potential of -19.9 ± 1.3 mV by dynamic light scattering (DLS) and surface charge measurements, and an average pore size of 15.3 ± 1.8 nm determined from cryogenic nitrogen adsorption isotherms using the Barrett-Joyner-Halenda (BJH) analysis of the adsorption/desorption isotherms (Figure 1b, Table 1 and Figure S1, Supporting Information). A comparison of hydrodynamic diameters of the pSiNPs after being subjected to the relevant immobilization chemistries showed that the particle size was maintained without significant aggregation of the nanoparticles (Figure 1b and Table S1, Supporting Information). To examine the effects of the trapping chemistries on the pSiNP hosts, we first carried

Table 1. Characteristics of pSiNP Pore Structures Determined from the Nitrogen Adsorption Isotherm Data

	Sample			
	pSiNPs	NH ₂ -pSiNPs	Ox-pSiNPs	Ca-pSiNPs
Surface area (m²/g) ^a	620 ± 31	545 ± 87	495 ± 79	409 ± 11
Pore volume $(cm^3/g)^b$	2.60 ± 0.22	1.63 ± 0.28	1.16 ± 0.24	0.80 ± 0.10
Pore size (nm) ^b	15.3 ± 1.8	13.4 ± 0.8	9.8 ± 0.4	8.8 ± 0.3

"Measured by nitrogen adsorption and determined using BET (Brunnauer–Emmett–Teller) analysis of the adsorption isotherms. "Measured by nitrogen adsorption and determined using BJH (Barrett–Joyner–Halenda) analysis of the adsorption/desorption isotherms. Reported values are the mean ± SD of the average pore diameter calculated from three measurements from three independently prepared samples.

out all of the chemistries on pSiNPs without incorporating Nluc in the synthesis process and compared the resulting nanostructures. Transmission electron microscope (TEM) images revealed different morphologies for the different trapping chemistries; the NH2-pSiNPs (Figure 1d and Figure S2b, Supporting Information) appeared similar to the asformed pSiNPs (Figure 1c and Figure S2a, Supporting Information), displaying a clearly discernible pore structure, whereas for both the Ox-pSiNPs (Figure 1e and Figure S2c, Supporting Information) and Ca-pSiNPs (Figure 1f and Figure S2d, Supporting Information) the pores appeared somewhat occluded. Analysis of the nitrogen adsorption data (Table 1 and Figure S1, Supporting Information) showed that all three chemistries led to reductions in apparent BET surface area, BJH pore volume and pore size, though both the Ox-pSiNPs and Ca-pSiNPs exhibited substantially lower values, as well as lower N₂ uptake capacities, than the NH₂-pSiNPs. From these data, we conclude that both the oxidation-induced encapsulation (Ox-pSiNPs) and calcium silicate-induced encapsulation (Ca-pSiNPs) methods fill the pores of the pSiNPs to some extent, with SiO₂ in the case of Ox-pSiNPs, and with a calcium silicate phase in the case of Ca-pSiNPs. As expected, the aminopropyldimethylethoxysilane chemistry of the NH₂pSiNPs led to coating of the pSiNP pore walls, but the monolayer surface coverage retained a relatively open pore morphology relative to the Ox-pSiNPs and Ca-pSiNPs encapsulation chemistries (Figure S1, Supporting Information). The purified Nluc was also prepared and characterized by SDS-PAGE and mass spectrometry (QTOF LC/MS) (see details in Table S2 and Figure S3, Supporting Information).

Next, the chemistries described above were used to immobilize the Nluc enzyme in the pSiNPs. This was accomplished for the Nluc@Ox-pSiNP and the Nluc@CapSiNP materials by premixing the Nluc protein with pSiNPs and then performing the relevant oxidative or calcium silicate trapping chemistries. For the Nluc@NH2-pSiNP control formulation, the protein was loaded into the NH2-pSiNPs after the surface amination chemistry had been performed. The average hydrodynamic diameters of the three Nluc@pSiNP constructs, measured after Nluc immobilization, were somewhat larger than the as-prepared pSiNPs (260-280 nm vs 210 nm, Table S1, Supporting Information). This study used a fixed nanoparticle size, and it did not explore the influence of overall nanoparticle size on catalytic performance. The zeta potential of the three Nluc@pSiNP constructs was also measured and compared to the corresponding controls, OxpSiNPs and Ca-pSiNPs and NH2-pSiNPs (Figure S4, Supporting Information). A noteworthy result is that both Nluc@Ox-pSiNPs and Nluc@Ca-pSiNPs displayed no significant shift in their zeta potential relative to the empty OxpSiNPs and Ca-pSiNPs, respectively (all displayed a zeta potential within 0.5 mV of -14.5 mV; Table S1). These data suggest that the encapsulation processes resulted in efficient encapsulation of Nluc in the nanoparticle pores and that the final surface charge of the Nluc@pSiNP constructs was regulated by the SiO₂ or calcium silicate coating at the nanoparticle surface. The zeta potential of the Nluc@NH₂pSiNP construct, by contrast, shifted from $+22.7 \pm 4.5$ mV to $+4.9 \pm 3.5$ mV after the immobilization process, suggesting the Nluc (which is negatively charged at pH 7) was primarily adsorbed at the particle surface. The encapsulation efficiency of each trapping chemistry was determined by using UV absorbance measurements of the supernatant at $\lambda = 280 \text{ nm}$

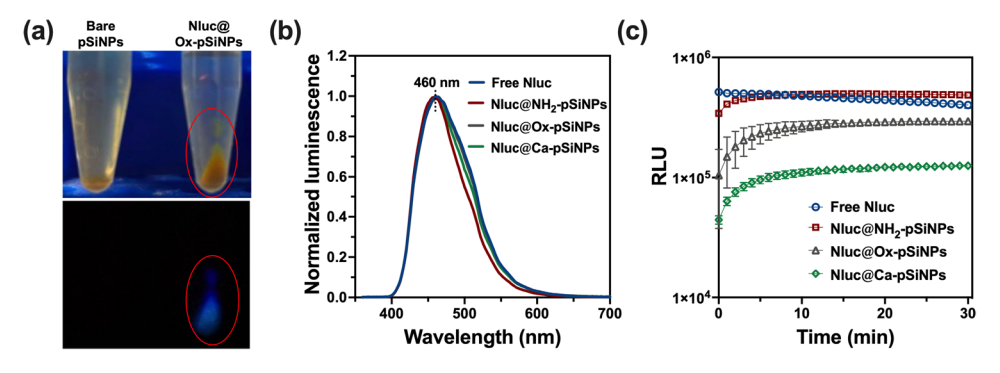


Figure 2. Chemiluminescence measurements from the catalytic reaction of Nano-Glo substrate with three different Nluc@pSiNP constructs. (a) Photographs of centrifuge tubes containing Nluc@Ox-pSiNPs (right) and empty pSiNP control nanoparticles (left), immersed in solutions containing the Nano-Glo assay reagents. Top: image taken under ambient light. Nanoparticles had been centrifuged prior to the photograph; the red circle indicates the region where nanoparticles are settled. Bottom: image taken in dark; blue is chemiluminescence from the assay. The assay was performed with Nluc (2.7 μM equivalent concentration) and Nano-Glo substrate prepared by a dilution of 100x from the stock in 1:1 (v:v) PBS/Nano-Glo buffer. (b) Normalized luminescence spectrum and (c) emission intensity as a function of time comparing free Nluc with the Nluc@pSiNP constructs. RLU = Relative Luminescence Units. The activity assays were performed at room temperature using the same effective concentration of Nluc at 7.5 nM and Nano-Glo substrate prepared by a 100× dilution of the stock solution in 1:1 (v:v) PBS/Nano-Glo buffer. Error bars indicate the standard deviation of three independent measurements from the three independently prepared samples.

and is summarized in Table S3. The mass loading of Nluc in the Nluc@pSiNP constructs was configured to be in the range 9-12% (w/w) by varying the enzyme concentration in the immobilization process. This was to avoid the possibility of compromising enzyme activity or stability that might have occurred upon overpacking of enzyme in the pores.^{34,35}

Characterization of Enzyme Activity in the Nluc@ **pSiNP** Constructs. To evaluate the performance of the enzyme trapped in the pSiNP constructs, a chemiluminescence-based assay using the commercially available Nano-Glo Luciferase System was performed. The Nano-Glo substrate, furimazine, is catalytically oxidized by Nluc, resulting in chemiluminescence that provides a convenient means to monitor enzyme activity. 31 As shown in Figure 2a for Nluc@ Ox-SiNPs, which had been separated from solution by centrifugation, chemiluminescence was localized at the nanoparticles. Similar results were observed for the other two Nluc@pSiNP constructs, indicating that all three approaches effectively immobilized the Nluc enzyme, while still allowing the enzyme to access its substrate. All three of the Nluc-loaded nanoparticle preparations could be pelletized by centrifugation and stored for up to 2 days without discernible loss in activity. For the electrostatically loaded Nluc@NH2-pSiNP formulation, leaching of Nluc was observed upon repeated washing steps (centrifugation followed by removal of supernatant and redispersion in fresh buffer), whereas the Nluc@Ox-pSiNP and Nluc@Ca-pSiNP constructs both retained their enzyme payloads under similar conditions (Figure S5, Supporting Information). The ready release of the Nluc enzyme from the Nluc@NH2-pSiNP construct is consistent with a simple, reversible, electrostatic binding process for this nanoparticle type. By contrast, the fact that Nluc was much more tightly held in the Nluc@Ox-pSiNPs and Nluc@Ca-pSiNPs is consistent with the conclusion that the Ox-pSiNP and CapSiNP chemistries trapped the Nluc essentially irreversibly within a mesoporous cage. Consequently, the more weakly surface-bound Nluc in the Nluc@NH2-pSiNP construct displayed higher activity and lower stability relative to the physically trapped Nluc of the Nluc@Ox-pSiNP and Nluc@ Ca-pSiNP constructs (vide infra).

Chemiluminescence assays indicated that the biological function of Nluc was preserved within the pSiNPs for all three constructs. The chemiluminescence spectra from free Nluc and the Nluc@pSiNP constructs are compared in Figure 2b. Under the same Nano-Glo assay conditions, Nluc@NH2-pSiNPs, Nluc@Ox-pSiNPs, and Nluc@Ox-pSiNPs all showed comparable wavelengths of maximum emission ($\lambda_{max} = 460 \text{ nm}$) and spectral lineshapes relative to free Nluc, consistent with the reported spectra of the Nano-Glo assay.³¹ The optical absorbance associated with each of the Nluc@pSiNP constructs was sufficiently low that it did not interfere with the luminescence measurements at the concentrations used in this assay (Figure S6, Supporting Information). Control experiments with empty pSiNPs (i.e., not loaded with Nluc) showed no luminescence under comparable conditions (Figure S7, Supporting Information).

The intensity of chemiluminescence produced from the Nluc@pSiNP constructs, which is correlated with the catalytic activity of Nluc, was studied and compared with free Nluc controls over a 30 min time course (Figure 2c). The concentration of Nluc used in the assay was 7.5 nM, and the initial concentration of substrate was set to be in large excess to achieve a sustained luminescence output (Figure S8, Supporting Information). For free Nluc, the maximum luminescence intensity was achieved immediately after the addition of the substrate, which was followed by a subsequent slow decay in intensity. This subsequent luminescence decay is indicative of substrate depletion due to the relatively high catalytic activity of the free Nluc enzyme. By contrast, all the Nluc@pSiNP constructs exhibited a slow increase in luminescence intensity at the initial stage of measurements and reached a plateau after approximately 10 min (Figure 2b). The steady-state intensity of chemiluminescence from the Nluc@Ox-pSiNP and Nluc@Ca-pSiNP constructs was lower than that of the free enzyme, and there were also significant differences between the three Nluc@pSiNP sample types: the most emissive construct was the Nluc@NH2-pSiNP control (where the Nluc was only weakly physisorbed to the nanoparticle surface), followed by the two caged formulations Nluc@Ox-pSiNPs and then Nluc@Ca-pSiNPs. This relative ordering of luminescence intensity implies reduced enzymatic

turnover for the caged enzyme. These differences could be attributed to a number of factors, including, but not limited to (1) the presence of orthosilicate, Ca (II), or other ions inhibiting Nluc activity; (2) denaturation of Nluc enzyme during loading—in particular, the Nluc@Ca-pSiNPs trapping chemistry was carried out at pH = 9; and (3) confinement in the pSiNP nanostructure causing hindered diffusion of the substrate and/or blockage of the Nluc active sites (for Nluc@Ox-pSiNPs and Nluc@Ca-pSiNPs). We next performed experiments to test these hypotheses.

Experiments testing the possibility that the enzyme was inhibited by the immobilization chemistry focused on orthosilicate and calcium(II) ions generated as the Ox-pSiNPs and Ca-pSiNPs dissolve in water. We carried out two control experiments examining activity of free Nluc after incubation in aqueous orthosilicate (0.6 mg/mL based on silicon) or CaCl_{2(aq)} (1M) for 1 h. The orthosilicate was prepared by first dissolving the as-etched pSiNPs in a borate buffer (pH = 10), and the pH of the solution was then adjusted to 7.4 by dilution with PBS (pH = 7.4). For the $CaCl_{2(aq)}$ experiments, the pH of the CaCl₂ solution was adjusted to pH 9, to best match the environment of the trapping process. The incubated enzymes were then diluted and subjected to the appropriate assay conditions. The luminescence assays showed negligible loss of Nluc activity (Figure S9a and S9b, Supporting Information). We note that the orthosilicate concentration used in these controls was an overestimate of the concentration of orthosilicate expected to be produced during the preparation of Nluc@Ox-pSiNPs, and the postencapsulation washing procedure removes residual orthosilicate or Ca (II) ions that may be present in the Nluc@pSiNPs preparations. Therefore, we conclude that the observed reduction of Nluc activity in the formulations of Nluc@OxpSiNPs and Nluc@Ca-pSiNPs cannot be attributed to inhibition by residual orthosilicate or Ca (II), or to enzyme denaturation under the pH 9 processing conditions.

Notably, chemiluminescence from Nluc@NH₂-pSiNPs required the least amount of time to reach a steady state intensity compared with the Nluc@Ox-pSiNPs and Nluc@Ca-pSiNPs, and its initial rate of photoemission was larger than observed in the assays of either the Nluc@Ox-pSiNPs or Nluc@Ca-pSiNPs. We interpret this result as an indication that Nluc in Nluc@NH₂-pSiNPs was more readily accessible to the substrate, consistent with the pore size, pore volume, and surface area measurements of these materials (Table 1). Of the two Nluc@Ox-pSiNP and Nluc@Ca-pSiNP constructs, the Nluc@Ca-pSiNPs displayed the smallest average pore size (Table 1) and the slowest rate of substrate turnover. These observations imply that hindered diffusion of the substrate within the pSiNP hosts plays a role in the resulting activity of encapsulated Nluc.

Effects of an Enzyme Inhibitor on Activity of the Nluc@pSiNP Constructs. To further evaluate the accessibility of the Nluc enzyme confined within the pSiNP nanostructure, we performed inhibition studies using a NanoLuc competitive inhibitor. The extracellular (cell-impermeable) inhibitor supplied by the manufacturer was used for these studies. In the inhibition assay, a fixed concentration of Nano-Glo substrate was preincubated with the Nluc@pSiNPs to generate the desired luminescence signal, and the decrease in luminescence intensity was then quantified as a function of the inhibitor concentration added to the assay. As shown in the dose—response curves of Figure 3a, Nluc@

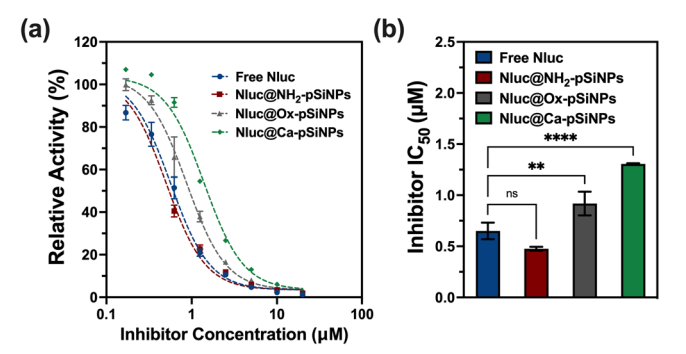


Figure 3. Dose-dependent inhibition of nanoluciferase activity by Nano-Glo extracellular inhibitor. (a) Dose-response curves for free Nluc, Nluc@NH2-pSiNPs, Nluc@Ox-pSiNPs, and Nluc@Ca-pSiNPs upon exposure to the indicated concentrations of Nano-Glo extracellular inhibitor (0-20 μ M). Curves are normalized to 100% relative activity at zero inhibitor concentrations for comparison. On an absolute scale, free Nluc displayed the highest activity at zero inhibitor concentration, followed by Nluc@NH2-pSiNPs, Nluc@OxpSiNPs, and then, Nluc@Ca-pSiNPs. (b) Half-maximal inhibitory concentrations, IC₅₀, calculated from the dose-response curves of (a) for free Nluc, Nluc@NH2-pSiNPs, Nluc@Ox-pSiNPs, and Nluc@CapSiNPs. All assays were performed at room temperature using the same effective concentration of Nluc at 7.5 nM, and the Nano-Glo substrate was prepared by a dilution of 100× from the stock in 1:1 (v:v) Nano-Glo buffer/PBS; the inhibitor compound at the indicated concentration was added to the assay wells that already contained the Nano-Glo substrate, and the samples were incubated for 5 min before the measurements. Error bars indicate the standard deviation of three independent measurements from three independently prepared samples. One-way ANOVA test was used for the data (**p < 0.01, ****p < 0.0001; n.s., not significant).

Ox-pSiNPs and Nluc@Ca-pSiNPs both required a higher concentration of inhibitor to reach the same level of activity compared to Nluc@NH₂-pSiNPs and free Nluc. The half-maximal inhibitory concentrations, IC₅₀, of each Nluc@pSiNP constructs and free Nluc are compared in Figure 3b. The larger IC₅₀ observed with Nluc@Ox-pSiNPs and Nluc@Ca-pSiNPs shows that encapsulation of the enzyme reduced the potency of the inhibitor

The results of Figure 3 confirm those of Figure 2c, indicating that confinement within the pSiNP host reduces the overall accessibility of the encapsulated Nluc guest to its substrate, be it the chemiluminescent precursor furimazine or its competitive inhibitor. However, the observed increase in the inhibitor's IC₅₀ for Nluc trapped in the nanoparticles relative to the IC₅₀ observed with free Nluc is not as obvious. The results indicate that the inhibitor molecule is less effective at accessing the interior of the nanoparticles than is furimazine. Here it is difficult to draw further conclusions, as the identity of the Nano-Glo substrate inhibitor in the assay kit are not given by the manufacturer. However, considering that it is marketed as an extracellular inhibitor that does not enter cells, it is likely that this inhibitor is a molecule similar to furimazine but containing a pendant sulfonate or other negatively charged group to inhibit cellular uptake.³⁶ The data of Figure 3b imply that the enzyme in the nanoconfined Nluc@Ca-pSiNPs (which displayed the smallest pore size, Table 1) was the least accessible to the inhibitor, followed by Nluc@Ox-pSiNPs. Since both of the caged nanoparticles under study displayed a net negative surface charge (Table S1), a negatively charged inhibitor would be expected to be at a lower effective

concentration inside the mesopores of the nanoparticles due to electrostatic repulsion. This would not be the case for the neutral furimazine molecule, which readily enters cells and should not be subject to the same electrostatic barrier when entering the nanoparticle cages. The main conclusion that can be drawn here is that the nanoparticle cages noticeably influence the accessibility of their guest enzymes to small probe molecules.

Protection of Nluc by Encapsulation. We next sought to assess the ability of the trapping chemistries to protect the enzyme under harsh environmental conditions. The Nluc enzyme is known to display broad stability in the pH range 5-9, with negligible loss in activity observed in the range from 7 to 9.31 Furthermore, as discussed above, the pSiNPs dissolve under basic conditions (particularly at pH > 10), complicating the evaluation of pH stability. Thus, for this work we chose to assess the protection afforded to Nluc by the trapping chemistries when subjected to high temperatures and when exposed to organic solvents. The free Nluc and Nluc@pSiNP constructs were subjected to temperatures ranging from 40 to 80 °C for 30 min, then cooled to room temperature and assessed for their catalytic activity. The results were compared to controls that were maintained at room temperature (RT, 25 ± 1 °C) throughout the experimental period (Figure 4 and

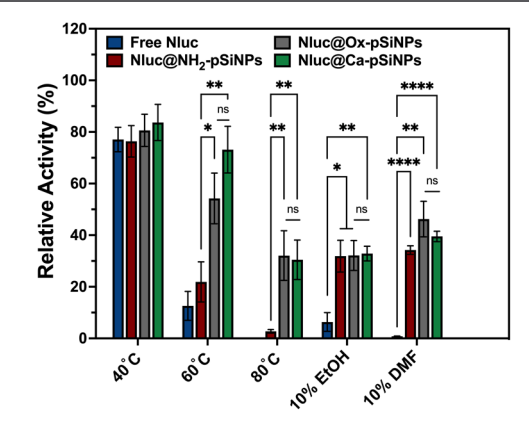


Figure 4. Relative activity of free Nluc and Nluc@pSiNP constructs after exposure to the indicated denaturing conditions. Each thermal denaturing condition (40 °C, 60 °C, and 80 °C) was run for 30 min, and the samples were allowed to cool to room temperature prior to evaluation of activity. All thermal treatments were performed in PBS (pH 7.4). The two solvent denaturing experiments were performed by placing the indicated construct in an aqueous mixture containing 10% by volume of either ethanol (10% EtOH) or dimethylformamide (10% DMF) for 30 min and then adding the assay reagents directly to the mixture. Activity assays were performed at room temperature using the same effective concentration of Nluc at 7.5 nM. Nano-Glo substrate was prepared by a 100x dilution from the stock using a 1:1 (v/v) Nano-Glo buffer/PBS. Error bars indicate the standard deviation of at least four measurements and are representative of three independently prepared samples. Tukey's multiple comparisons test was used for the data (*p < 0.05, **p < 0.01, ****p < 0.0001; n.s., not significant).

Figure S10, Supporting Information). Consistent with the known denaturation behavior of the enzyme, the activity of free Nluc decreased substantially after incubation at 60 °C, and the enzyme was completely inactivated by treatment at 80 °C.³¹ Both of the formulations in which Nluc was physically trapped (Nluc@Ox-pSiNPs and Nluc@Ca-pSiNPs) showed superior thermal stability compared to Nluc@NH₂-pSiNPs

after incubation at 60 and 80 °C (Figure 4). This latter construct was the one for which the enzymes were only loosely adsorbed, bound by electrostatic interactions rather than physical trapping. The low thermal stability of Nluc@NH₂-pSiNPs is attributed to the immobilization chemistry; the loosely bound Nluc in NH₂-pSiNPs is more susceptible to thermal denaturation. Both Nluc@Ox-pSiNPs and Nluc@Ca-pSiNPs showed substantial preservation of enzyme activity following the 60 and 80 °C thermal treatments, and there were no significant differences between the two (Table S4, Supporting Information).

We attribute the ability of the mesoporous nanoparticle hosts to suppress thermal denaturation of the enzyme to nanoscale interactions between the unfolding protein and its cage. Presumably, the nanoconfinement prevents the thermally unfolded protein from aggregating with other proteins as the system cools, a mechanism that governs the irreversible thermal denaturation of most proteins. Most likely the trapped enzymes still unfold at 80 °C, but being trapped in the nanocages, aggregation and detrimental polypeptide chain dynamics are prevented, allowing the enzyme to refold upon cooling. This is reminiscent of the natural GroES/GroEL chaperone system, which helps protein folding *in vivo* by a similar mechanism of nanoconfinement.

The resistance of the Nluc@pSiNP constructs to organic solvents was evaluated by exposing them to aqueous solutions of denaturing organic solvents. When exposed to either 10% (by volume) ethanol (EtOH) or dimethylformamide (DMF) in PBS (pH 7.4), significant retention of activity (30–45%) was observed regardless of the immobilization chemistry used (Figure 4). By contrast, free Nluc exhibited a significant and substantial reduction in activity upon exposure to either solvent (Figures S11 and S12, Supporting Information). The resistance to denaturation by organic solvents was not particularly dependent on the type of Nluc@pSiNP construct used to host the Nluc payload; the two caged formulations performed similarly to the surface-adsorbed control Nluc@ NH₂-pSiNP. This may be due to the mechanism of enzyme deactivation; in addition to causing protein unfolding, organic solvents deactivate enzymes by penetrating into their active sites, removing critically important waters of hydration, and rigidifying the enzyme conformation.³⁹ Although confinement in the nanostructure might reduce the tendency of the enzyme to unfold and aggregate, it is not likely to prevent the penetration of solvent molecules. Indeed, the fact that the furimazine substrate could enter the nanostructure and be processed by the enzyme implies that the smaller ethanol or dimethylformamide molecules could also readily enter the region where the enzyme resides in the caged formulations. The main conclusion that can be drawn here is that the pSiNP cages impart substantial resistance both to polar organic solvents and to thermal denaturing conditions when compared with the free enzyme.

Cellular Uptake and Retention of Enzyme Activity in Cells. The Nluc enzyme is typically deployed as a genetic reporter, to elucidate particular cellular processes or to assess gene expression within cells.³⁰ For these purposes, it is introduced to the cells via a genetic vector that encodes for the bioluminescent reporter protein NLuc, which is then synthesized *in situ*. The NLuc protein has not previously been incorporated into a nanoparticle as a reporter. So in this work, we assessed the compatibility of the Nluc-loaded pSiNP cages with a cellular assay, to see if the enzyme constructs

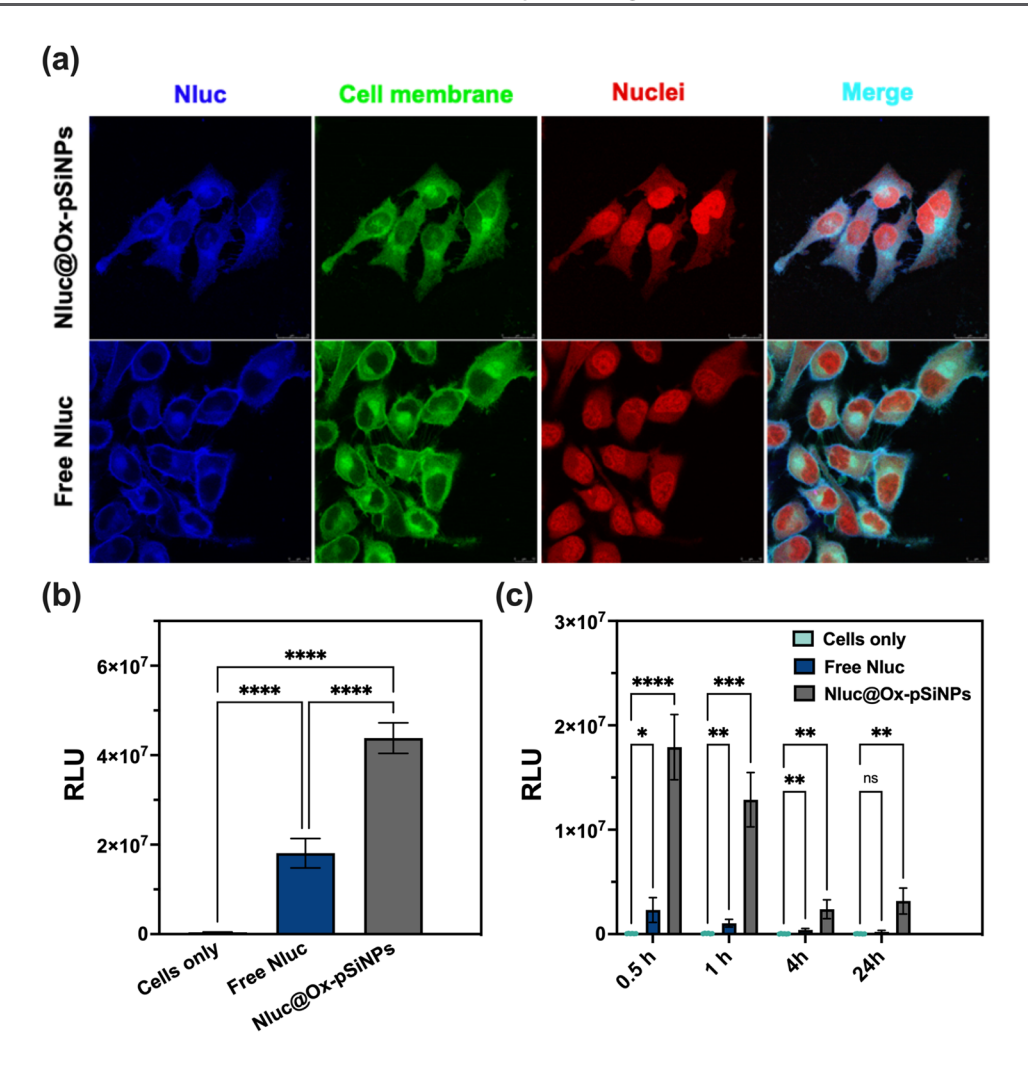


Figure 5. Cell retention and enzyme activity of Nluc@Ox-pSiNPs and free Nluc in the presence of HeLa cells. (a) Representative microscope images of Hela cells after incubation with Nluc@Ox-pSiNPs or free Nluc at 37 °C for 30 min. In either experiment, cells were treated using the same effective concentration of Nluc (3 μ g/mL), in an Opt-MEM medium in a 5% CO₂ atmosphere. Cells were then fixed with 4% PFA and transferred to glass slides, and stained with CellMask plasma membrane stain (green channel) and NucRed Live 647 ReadyProbes nuclear stain (red channel). Cell membrane and nuclear stains were imaged in a confocal mode; the nanoluciferase (Nluc) images (blue) were acquired in a chemiluminescence imaging mode (no laser excitation), 10 min after addition of the Nano-Glo substrate to induce luminescence. (b) Relative luminescence intensity generated from HeLa cells incubated with Nluc@Ox-pSiNPs or free Nluc for 30 min, then rinsed to remove excess nanoparticles or enzyme, then treated with the Nano-Glo substrate to induce luminescence. Free cells, with no luminogenic reagents added, are shown as a control. Cell preparations are as in (a), except the cells were not fixed or stained prior to the chemiluminescence assay, which was performed in a microplate reader. (c) Comparison of relative chemiluminescence intensity emitted from HeLa cell cultures as a function of time. Cells were incubated with Nluc@Ox-pSiNPs or free Nluc for 30 min as above, washed with buffer to remove unbound nanoparticles or enzyme, then incubated for the indicated times. Cells were then rinsed again, treated with the Nano-Glo substrate + buffer, and luminescence was quantified (λ = 460 nm) 10 min later. Data in (b) and (c) represent mean ± SD of n = 6 replicates, and statistical significance was calculated using two-way ANOVA; *p < 0.005, **p < 0.001, ****p < 0.0001; n.s., not significant).

could be retained by cells and still maintain their function under standard cell culture conditions. For these studies, the oxidation-induced trapping chemistry (Nluc@Ox-pSiNPs) was used. Human cervical carcinoma (Hela) cells were treated with either Nluc@Ox-pSiNPs or free Nluc at the same effective concentration of Nluc for 30 min, and their cellular retention and enzymatic activity were assessed using both confocal microscopy of fixed cells and on live cells monitored over a 24-h period using a microplate format. After incubation, the cells were rinsed with fresh buffer to remove excess free enzyme or nanoparticle construct from the media. The microscope images confirmed that after a 30 min incubation period both Nluc@Ox-pSiNPs and free Nluc are retained by the cells. The characteristic blue chemiluminescence from the enzyme

reaction on its substrate was observed from the cells in either case (Figure 5a). However, the intensity of chemiluminescence was significantly lower for the free enzyme compared to that of the Nluc@Ox-pSiNPs (Figure 5b).

Cells treated with the enzyme-loaded nanoparticles also retained the enzyme and its activity for a substantially longer period of time compared with that of the free Nluc enzyme, indicating that the HeLa cells retained substantially greater quantities of the enzyme when it was delivered in the nanoparticle carrier. For this purpose, the cells were first treated with Nano-Glo Luciferase assay buffer containing detergents to induce cell lysis prior to the enzyme activity assay. This was done to ensure similar access of the furimazine substrate to either the nanoparticle-bound or free forms of the

enzyme; for example, if the Nluc@Ox-pSiNPs had been internalized, while free Nluc was retained at the surface of the cellular membrane, the intensity of chemiluminescence might have been affected by the rate of cellular internalization of the furimazine substrate. The luminescence generated from Nluc@ Ox-pSiNPs was substantial after 24 h of incubation with the cells, whereas the luminescence generated from the group treated with free Nluc was not significantly above the noise level at this time point (Figure 5c). These data demonstrate that the pSiNP cage retained the function of the encapsulated enzyme under the cellular incubation and assay conditions, and it also suggests that the nanoparticles facilitated intracellular uptake of Nluc. The present study did not evaluate uptake pathways or the mechanism(s) of cellular retention of the nanoparticles, though it is likely the Nluc@Ox-pSiNPs entered into cells via an endocytic pathway. 40 Further studies are needed to determine if the nanocages can mitigate the hydrolytic and proteolytic degradation processes associated with endocytosis.

CONCLUSIONS

Encapsulation of the enzyme nanoluciferase within mesoporous silicon nanoparticle cages was achieved by using oxidation-induced trapping (Ox-pSiNP) and calcium silicate condensation (Ca-pSiNP) chemistries. The enzyme retained its biological function, and it exhibited an ability to turn over substrate while still confined within either nanoparticle host. Activity of the enzyme entrapped in the two formulations was lower than for controls involving the free enzyme or the enzyme simply bound electrostatically to the porous silicon nanoparticle surface rather than trapped within a nanoparticle cage. The activity of the immobilized enzyme correlated with the open pore size and, by inference, the accessibility of the substrate to the enzyme trapped within the nanoparticle cages. Due to lower substrate turnover rates, the enzyme trapped in Ox-pSiNP and Ca-pSiNP cages also showed prolonged chemiluminescence emission relative to the free enzyme. The two trapping chemistries appeared to behave as encapsulants that secured the enzyme within the host with minimal leakage compared to the electrostatically bound control, which readily leached the enzyme from the nanoparticle host. These trapping chemistries also imparted stability to the enzyme when exposed to elevated temperatures or to organic solvents, with the oxidation-induced encapsulation chemistry (Ox-pSiNP) showing higher catalytic activity, which was attributed to its slightly more open and accessible mesoporous nanostructure. Both of these caged nanoparticles imparted substantial protection against thermal denaturation compared to the free enzyme or to a surface-bound enzyme control. Finally, the suitability of the enzyme-cage nanostructure as a cellular reporter was evaluated. The Nluc-loaded Ox-pSiNP formulation was found to be retained by HeLa human cervical carcinoma cells, and its catalyzed chemiluminescence property was preserved through both live incubation and fixing conditions. This work provides a blueprint for the design of porous nanoparticles that can act as host materials for immobilized guest biologics, which could expand their utility in catalysis, in enzymatic sensing or in cellular reporter systems.

■ EXPERIMENTAL SECTION

Materials. Single-crystal highly doped p-type (B-doped) silicon wafers of resistivity 0.8-1 m Ω -cm, polished on the (100) face, were

purchased from Siltronix Corp. Calcium Chloride (CaCl₂) was purchased from Sigma-Aldrich. 3-Aminopropyldimethylethoxysilane (APDMES) was purchased from Gelest, Inc. Nano-Glo luciferase assay substrate and inhibitor (Cat #: N1110 and N2162) were purchased from Promega, USA. Other chemicals or reagents used were of analytic grade and used without further purification. HeLa cells and EMEM (Eagle's Minimum Essential Medium) were obtained from ATCC (www.atcc.org). Fetal bovine serum was purchased from MilliporeSigma. L-Glutamine, Penicillin—Streptomycin, and Opti-MEM, Nunc Lab-Tek II Chamber Slide System, CellMask Plasma Membrane Stains, NucRed Live 647 ReadyProbes Reagent, and ProLong Diamond Antifade Mountant were purchased from ThermoFisher Scientific.

Preparation of pSiNPs. The pSiNPs with an approximate diameter of 200 nm were prepared using an electrochemical perforation etching method described previously.³³ Briefly, a singlecrystal Si wafer was diced into a square of approximately 5 cm × 5 cm and mounted in a Teflon etching cell. The O-ring seal of the cell exposed 9.6 cm² of the Si surface to electrolyte. The chip was contacted on the backside with aluminum foil, and the wafer was electrochemically anodized using a platinum coil counter-electrode in an electrolyte consisting of 3:1 (v:v) 48% aqueous hydrofluoric acid (HF):ethanol (CAUTION: HF is highly toxic and can cause severe burns on contact with the skin or eyes). Prior to preparation of the porous layers, the chip was cleaned using a "sacrificial etch" which consisted of etching a thin porous Si layer into the chip (50 mA·cm⁻² applied for 60 s) in the above electrolyte, removing the electrolyte, rinsing the cell with ethanol, and then dissolving this layer in a strong base (2 M aqueous KOH). The perforation etch was performed by applying a current density of 50 mA·cm⁻² for 4.18 s followed by 335 mA·cm⁻² for 0.363 s. This waveform was repeated for 150 cycles, generating a porous Si film with alternating layers of high and low porosity. The resulting porous silicon layer was rinsed with ethanol several times and then lifted off the substrate by application of a current density of 4 mA·cm⁻² for 250 s in an electrolyte consisting of 1:20 (v:v) 48% aqueous HF:ethanol. The etching cell containing the free-standing porous Si film was then thoroughly rinsed with ethanol and collected in a glass vial before further use. For a typical nanoparticle preparation, four free-standing porous Si films were combined in a glass vial with 10 mL of deionized water and ultrasonicated for 18 h. The brown suspension collected after the ultrasonication was centrifuged at 15,000 rpm for 10 min, and the pellets were collected and the supernatant was decanted. The pellets were then rinsed by successive centrifugation and resuspension in ethanol for three times to remove the smaller size fraction of particles. Next, the particles were centrifuged at 2000 rpm for 3 min and the supernatant was collected to remove the large particles. The suspension was stored in ethanol at room temperature until further use. To determine the nanoparticle concentration in these suspensions, 500 μ L fractions of the particle suspension were centrifuged at 15,000 rpm and the supernatants were decanted, followed by drying the pellets under vacuum. Eppendorf tubes were weighed before adding the solution and after the vacuum-dry process, and the nanoparticle mass was determined from the weight difference. This procedure typically yielded 0.6 mg of pSiNPs.

Nanoluciferase (Nluc) Loading via Amine Electrostatic Adsorption. 0.6 mg amount of pSiNPs was first suspended in a 1% (v/v) solution of 3-aminopropyldimethylethoxysilane (APDMES) in ethanol and agitated on a vortex mixer for 2 h at room temperature to graft terminal amines on the nanoparticle surface. Following the reaction, the aminated nanoparticles were rinsed by successive centrifugation and redispersion in ethanol three times. For Nluc loading, 0.6 mg aminated pSiNPs were suspended in 1 mL Nluc solution (120 μ g·mL⁻¹ in deionized water) and agitated on a rotating mixer at 4 °C for 2 h. The Nluc-loaded pSiNPs were then pelletized by centrifugation for 10 min at 15,000 rpm, washed 2X with DI water by successive redispersion/centrifugation for 10 min at 15,000 rpm steps, and the loading and washing solutions were collected for quantification of encapsulation efficiency (EE%). Nluc EE% was calculated from the initial and final concentrations of the loading and

washing solutions (n=3) determined from the UV absorbance at 280 nm. The final nanoparticles were pelletized by centrifugation and removal of the buffer solution, and they were stored for up to 2 days at 4 °C prior to testing.

Nanoluciferase (Nluc) Loading via Oxidation-Induced Encapsulation. The method was adapted from a published route. 32 0.6 mg of as-etched pSiNPs were suspended in 1 mL Nluc solution ($60 \mu g \cdot mL^{-1}$ in 1× phosphate-buffered saline, pH = 7.4) and agitated on a rotating mixer at 4 °C for ~18 h. The Nluc-loaded pSiNPs were then centrifuged for 10 min at 15,000 rpm, washed 2× with PBS by successive centrifugation for 10 min at 15,000 rpm and redispersion, and the loading and washing solutions were collected for quantification of encapsulation efficiency (EE%). Nluc EE% was calculated from the initial and final concentrations of the loading and washing solutions (n = 3) determined from the UV absorbance at 280 nm. The final nanoparticles were pelletized by centrifugation and removal of the buffer solution, and they were stored for up to 2 days at 4 °C prior to testing.

Nanoluciferase (Nluc) Loading via Calcium Silicate-Induced **Encapsulation.** A stock solution of 2 M calcium chloride (CaCl₂) was prepared in RNase-free water. The solution was centrifuged to remove any precipitates. For Nluc loading, Nluc was resuspended in RNase-free water at a concentration of 120 μ g·mL⁻¹ and 500 μ L of Nluc solution was mixed with 0.6 mg of pSiNPs. This solution was then mixed with 500 µL of 2 M CaCl₂ solution, giving a final concentration of 60 μg·mL⁻¹ Nluc, 0.6 mg·mL⁻¹ pSiNPs, and 1 M CaCl2 in 1 mL of RNase-free water. The solution was agitated on a rotating mixer at 4 °C for 1 h. The Nluc-loaded pSiNPs were then centrifuged for 10 min at 15,000 rpm, washed 2× with PBS by successive centrifugation for 10 min at 15,000 rpm and redispersion, and the loading and washing solutions were collected for quantification of encapsulation efficiency (EE%). Nluc EE% was calculated from the initial and final concentrations of the loading and washing solution (n = 3) determined from the UV absorbance at 280 nm. The final nanoparticles were pelletized by centrifugation and removal of the buffer solution, and they were stored for up to 2 days at 4 °C prior to testing.

Materials Characterization. TEM images were obtained with a JEOL-5 1200 EX II 120 kV instrument. Hydrodynamic size and zeta potential were measured by dynamic light scattering (DLS) using a Zetasizer ZS90 instrument (Malvern Instruments). Nitrogen adsorption—desorption isotherms were obtained on dry particles at a temperature of 77 K with a Micromeritics ASAP 202 instrument. UV absorbance measurements to quantify protein concentrations were performed on a NanoDrop 2000 spectrophotometer (Thermo Fisher Scientific).

Evaluation of Catalytic Performance of Nluc and Nluc@pSiNP Constructs by Nano-Glo Assay. A 96-well plate reader (SpectraMax iD5 plate reader, Molecular Devices) was used to monitor enzyme activity through the generation of luminescence (quantified as RLU, or Relative Luminescence Units), measured at a wavelength of 460 nm, immediately after the addition of samples to a Nano-Glo substrate solution. Nano-Glo substrates (1:49 v:v dilution in Nano-Glo buffer, 50 μ L) were loaded into the wells of the 96-well plate, and then free Nluc or Nluc-loaded pSiNPs (50 μ L in PBS) were added to the substrate solution using a multichannel pipet to achieve a final enzyme concentration of ~7.5 nM. For each sample, three replicates were measured in three separate wells in parallel. The final data were analyzed in triplicate from three independent batches.

Confocal Imaging of Cell Internalization of Nluc@OxpSiNPs and Nluc. Hela cells were obtained from the American Type Culture Collection (ATCC), cultured in EMEM supplemented with 10% FBS, 5% L-Glutamine, and 5% penicillin–streptomycin, and maintained at 37 °C in a 5% CO₂ atmosphere. In a typical experiment, the cells were plated in an 8-well Nunc-Lab Tek chamber at a density of 10^5 cells per well and allowed to adhere overnight. The cells were then treated with Nluc@Ox-pSiNPs or free Nluc at the same effective concentration of Nluc (3 μ g/mL) in Opti-MEM at 37 °C for 30 min, and then the wells were rinsed three times with 1X PBS. The cells were then fixed with 4% formaldehyde for 5 min. Cell membranes and

nuclei were stained with Cell Mask Plasma Membrane stain and NucRed Live 647 Ready Probes, respectively. Following the staining, Nano-Glo substrate was added to generate the luminescence from Nluc@Ox-pSiNPs and Nluc. A coverslip was mounted using Prolong Diamond Antifade Mountant, and the imaging was performed using a Leica SPE confocal microscope. Note that the chemiluminescent signal from the NanoLuc was obtained by reducing the laser power to zero and capturing the image with a 450 nm band-pass filter using the same confocal microscope.

Enzyme Activity of Nluc@Ox-pSiNPs and Nluc after Internalization by Cells. Hela cells were plated in clear, flatbottom 96-well plates at a density of 4×10^4 cells per well. After 24 h, the cells were treated with Nluc@Ox-pSiNPs or free Nluc in Opti-MEM media, using the same effective concentration of Nluc (3 $\mu g/$ mL) for 30 min at 37 °C and washed with 1X PBS three times to remove excess particles or free enzyme. The cells were then incubated in EMEM supplemented with 10% FBS, 5% L-Glutamine, and 5% penicillin-streptomycin at 37 °C in a 5% CO2 atmosphere for the relevant time period (between 0.5 and 24 h), at which point they were assayed in luminescence mode on the plate reader. For each set of cells being assayed at a given time point, the wells were first washed one time with PBS, then 100 μ L of Nano-Glo substrate in Nano-Glo buffer (1:200 v:v dilution) was added to lyse the cells and initiate chemiluminescence. The samples were then incubated at 37 °C for 10 min and the luminescence intensity was quantified at a wavelength of

ASSOCIATED CONTENT

Supporting Information

The Supporting Information is available free of charge at https://pubs.acs.org/doi/10.1021/acs.chemmater.3c02637.

Nitrogen adsorption/desorption isotherms of the pSiNPs, NH₂-pSiNPs, Ox-pSiNPs, and Ca-pSiNPs; Hydrodynamic size and zeta potential for the different pSiNP and Nluc@pSiNP constructs; Encapsulation efficiency and mass loading of Nluc using different pSiNP constructs; Nluc leaching curves; Absorbance spectra of NH₂-pSiNPs, Ox-pSiNPs, and Ca-pSiNPs; Emission intensity as a function of time of NH₂-pSiNPs, Ox-pSiNPs, and Ca-pSiNPs; Emission intensity as a function of time of free Nluc at the concentration of 2.5-75 nM; Emission intensity as a function of time of free Nluc before and after treating with CaCl2 and orthosilicate solution; Emission intensity as a function of time of free Nluc, Nluc@NH2-pSiNPs, Nluc@OxpSiNPs, and Nluc@Ca-pSiNPs after thermal treatment; Emission intensity as a function of time of free Nluc in the presence of ethanol and dimethylformamide at varying concentrations (5-50%, v/v); and Emission intensity as a function of time of Nluc@NH2-pSiNPs, Nluc@Ox-pSiNPs, and Nluc@Ca-pSiNPs after treating with ethanol and dimethylformamide (10% by volume) (PDF)

AUTHOR INFORMATION

Corresponding Author

Michael J. Sailor — Materials Science and Engineering Program and Department of Chemistry and Biochemistry, University of California, San Diego, La Jolla, California 92093, United States; orcid.org/0000-0002-4809-9826; Email: msailor@ucsd.edu

Authors

- Yi-Sheng Lu Materials Science and Engineering Program, University of California, San Diego, La Jolla, California 92093, United States
- Ruhan Fan Materials Science and Engineering Program, University of California, San Diego, La Jolla, California 92093, United States; orcid.org/0000-0003-0626-849X
- Willem Vugs Department of Biomedical Engineering and Institute for Complex Molecular Systems (ICMS), Eindhoven University of Technology, 5600 MB Eindhoven, The Netherlands
- Lieuwe Biewenga Department of Biomedical Engineering and Institute for Complex Molecular Systems (ICMS), Eindhoven University of Technology, 5600 MB Eindhoven, The Netherlands
- Ziming Zhou Department of Chemistry and Biochemistry, University of California, San Diego, La Jolla, California 92093, United States; Oorcid.org/0000-0002-2973-576X
- Sanahan Vijayakumar Materials Science and Engineering Program, University of California, San Diego, La Jolla, California 92093, United States
- Maarten Merkx Department of Biomedical Engineering and Institute for Complex Molecular Systems (ICMS), Eindhoven University of Technology, 5600 MB Eindhoven, The Netherlands; orcid.org/0000-0001-9484-3882

Complete contact information is available at: https://pubs.acs.org/10.1021/acs.chemmater.3c02637

Notes

The authors declare the following competing financial interest(s): MJS is a scientific founder (SF), member of the Board of Directors (BOD), Advisory Board (AB), Scientific Advisory Board (SAB), acts as a paid consultant (PC) or has an equity interest (EI) in the following: Aivocode, Inc (AB, EI); Bejing ITEC Technologies (SAB, PC); Lisata Therapeutics (EI); Illumina (EI), Matrix Technologies (EI); NanoVision Bio (SAB, EI); Precis Therapeutics (SF, BOD, EI), Quanterix (EI), Spinnaker Biosciences, Inc. (SF, BOD, EI); TruTag Technologies (SAB, EI); and Well-Healthcare Technologies (SAB, PC). Although one or more of the grants that supported this research has been identified for conflict of interest management based on the overall scope of the project and its potential benefit to the companies listed, the research findings included in this publication may not necessarily relate to their interests. The terms of these arrangements have been reviewed and approved by the University of California, San Diego in accordance with its conflict of interest policies.

ACKNOWLEDGMENTS

We thank Dr. Simone Wouters for providing initial support of this project. This research was primarily supported by NSF through the UC San Diego Materials Research Science and Engineering Center (UCSD MRSEC), DMR-2011924. Additional support provided from the NIH through grant R01 AI132413-01 and from the Defense Advanced Research Projects Agency (DARPA) and Naval Information Warfare Center Pacific, (NIWC Pacific) under Contract No. N66001-21-C-4010. Any opinions, findings and conclusions or recommendations expressed in this material are those of the author(s) and do not necessarily reflect the views of the DARPA or NIWC Pacific. The authors acknowledge the use of facilities and instrumentation supported by the National

Science Foundation through the UC San Diego Materials Research Science and Engineering Center (UCSD MRSEC) DMR-2011924, and by the San Diego Nanotechnology Infrastructure (SDNI) of UCSD, a member of the National Nanotechnology Coordinated Infrastructure, which is supported by the National Science Foundation (Grant ECCS-2025752).

REFERENCES

- (1) Vriezema, D. M.; Comellas Aragonès, M.; Elemans, J. A. A. W.; Cornelissen, J. J. L. M.; Rowan, A. E.; Nolte, R. J. M. Self-Assembled Nanoreactors. *Chem. Rev.* **2005**, *105* (4), 1445–1490.
- (2) Kao, K.-C.; Lin, T.-S.; Mou, C.-Y. Enhanced Activity and Stability of Lysozyme by Immobilization in the Matching Nanochannels of Mesoporous Silica Nanoparticles. *J. Phys. Chem. C* **2014**, *118* (13), 6734–6743.
- (3) Cui, J.; Tan, Z.; Han, P.; Zhong, C.; Jia, S. Enzyme Shielding in a Large Mesoporous Hollow Silica Shell for Improved Recycling and Stability Based on CaCO₃ Microtemplates and Biomimetic Silicification. *J. Agric. Food Chem.* **2017**, *65* (19), 3883–3890.
- (4) Sun, Q.; Fu, C.-W.; Aguila, B.; Perman, J.; Wang, S.; Huang, H.-Y.; Xiao, F.-S.; Ma, S. Pore Environment Control and Enhanced Performance of Enzymes Infiltrated in Covalent Organic Frameworks. *J. Am. Chem. Soc.* **2018**, *140* (3), 984–992.
- (5) Li, P.; Moon, S.-Y.; Guelta, M. A.; Harvey, S. P.; Hupp, J. T.; Farha, O. K. Encapsulation of a Nerve Agent Detoxifying Enzyme by a Mesoporous Zirconium Metal—Organic Framework Engenders Thermal and Long-Term Stability. *J. Am. Chem. Soc.* **2016**, *138* (26), 8052–8055.
- (6) Liang, W.; Carraro, F.; Solomon, M. B.; Bell, S. G.; Amenitsch, H.; Sumby, C. J.; White, N. G.; Falcaro, P.; Doonan, C. J. Enzyme Encapsulation in a Porous Hydrogen-Bonded Organic Framework. *J. Am. Chem. Soc.* **2019**, *141* (36), 14298–14305.
- (7) Liang, W.; Xu, H.; Carraro, F.; Maddigan, N. K.; Li, Q.; Bell, S. G.; Huang, D. M.; Tarzia, A.; Solomon, M. B.; Amenitsch, H.; Vaccari, L.; Sumby, C. J.; Falcaro, P.; Doonan, C. J. Enhanced Activity of Enzymes Encapsulated in Hydrophilic Metal—Organic Frameworks. J. Am. Chem. Soc. 2019, 141 (6), 2348—2355.
- (8) Muntimadugu, E.; Silva-Abreu, M.; Vives, G.; Loeck, M.; Pham, V.; del Moral, M.; Solomon, M.; Muro, S. Comparison between Nanoparticle Encapsulation and Surface Loading for Lysosomal Enzyme Replacement Therapy. *Int. J. Mol. Sci.* **2022**, 23 (7), 4034.
- (9) Zhuang, J.; Duan, Y.; Zhang, Q.; Gao, W.; Li, S.; Fang, R. H.; Zhang, L. Multimodal Enzyme Delivery and Therapy Enabled by Cell Membrane-Coated Metal—Organic Framework Nanoparticles. *Nano Lett.* **2020**, 20 (5), 4051–4058.
- (10) Cases Díaz, J.; Lozano-Torres, B.; Giménez-Marqués, M. Boosting Protein Encapsulation through Lewis-Acid-Mediated Metal-Organic Framework Mineralization: Toward Effective Intracellular Delivery. *Chem. Mater.* **2022**, 34 (17), 7817–7827.
- (11) Chen, M.; Zeng, G.; Xu, P.; Lai, C.; Tang, L. How Do Enzymes 'Meet' Nanoparticles and Nanomaterials? *Trends Biochem. Sci.* **2017**, 42 (11), 914–930.
- (12) Majewski, M. B.; Howarth, A. J.; Li, P.; Wasielewski, M. R.; Hupp, J. T.; Farha, O. K. Enzyme encapsulation in metal—organic frameworks for applications in catalysis. *CrystEngComm* **2017**, *19* (29), 4082–4091.
- (13) Chapman, R.; Stenzel, M. H. All Wrapped up: Stabilization of Enzymes within Single Enzyme Nanoparticles. *J. Am. Chem. Soc.* **2019**, 141 (7), 2754–2769.
- (14) Zuidema, J. M.; Dumont, C. M.; Wang, J.; Batchelor, W. M.; Lu, Y.-S.; Kang, J.; Bertucci, A.; Ziebarth, N. M.; Shea, L. D.; Sailor, M. J. Porous Silicon Nanoparticles Embedded in Poly(lactic-coglycolic acid) Nanofiber Scaffolds Deliver Neurotrophic Payloads to Enhance Neuronal Growth. *Adv. Funct. Mater.* **2020**, 30 (25), No. 2002560.
- (15) Beavers, K. R.; Werfel, T. A.; Shen, T.; Kavanaugh, T. E.; Kilchrist, K. V.; Mares, J. W.; Fain, J. S.; Wiese, C. B.; Vickers, K. C.;

- Weiss, S. M.; Duvall, C. L. Porous Silicon and Polymer Nano-composites for Delivery of Peptide Nucleic Acids as Anti-MicroRNA Therapies. *Adv. Mater.* **2016**, *28* (36), 7984–7992.
- (16) Thomas, J. C.; Pacholski, C.; Sailor, M. J. Delivery of Nanogram Payloads Using Magnetic Porous Silicon Microcarriers. *Lab Chip* **2006**, *6* (6), 782–787.
- (17) Turner, C. T.; McInnes, S. J. P.; Melville, E.; Cowin, A. J.; Voelcker, N. H. Delivery of Flightless I Neutralizing Antibody from Porous Silicon Nanoparticles Improves Wound Healing in Diabetic Mice. *Adv. Healthc. Mater.* **2017**, *6* (2), No. 1600707.
- (18) Kong, F.; Zhang, H.; Qu, X.; Zhang, X.; Chen, D.; Ding, R.; Mäkilä, E.; Salonen, J.; Santos, H. A.; Hai, M. Gold Nanorods, DNA Origami, and Porous Silicon Nanoparticle-functionalized Biocompatible Double Emulsion for Versatile Targeted Therapeutics and Antibody Combination Therapy. *Adv. Mater.* **2016**, *28* (46), 10195–10203.
- (19) Kang, J.; Joo, J.; Kwon, E. J.; Skalak, M.; Hussain, S.; She, Z.-G.; Ruoslahti, E.; Bhatia, S. N.; Sailor, M. J. Self-Sealing Porous Silicon-Calcium Silicate Core—Shell Nanoparticles for Targeted siRNA Delivery to the Injured Brain. *Adv. Mater.* **2016**, 28 (36), 7962—7969.
- (20) Wang, J.; Kumeria, T.; Bezem, M. T.; Wang, J.; Sailor, M. J. Self-Reporting Photoluminescent Porous Silicon Microparticles for Drug Delivery. ACS Appl. Mater. Interfaces 2018, 10 (4), 3200–3209.
- (21) Takahashi, H.; Li, B.; Sasaki, T.; Miyazaki, C.; Kajino, T.; Inagaki, S. Catalytic Activity in Organic Solvents and Stability of Immobilized Enzymes Depend on the Pore Size and Surface Characteristics of Mesoporous Silica. *Chem. Mater.* **2000**, *12* (11), 3301–3305.
- (22) Wang, X.; Lan, P. C.; Ma, S. Metal-Organic Frameworks for Enzyme Immobilization: Beyond Host Matrix Materials. *ACS Cent. Sci.* **2020**, *6* (9), 1497–1506.
- (23) Zhao, F.; Liu, H.; Mathe, S. D. R.; Dong, A.; Zhang, J. Covalent Organic Frameworks: From Materials Design to Biomedical Application. *Nanomaterials* **2018**, *8* (1), 15.
- (24) Ettlinger, R.; Lächelt, U.; Gref, R.; Horcajada, P.; Lammers, T.; Serre, C.; Couvreur, P.; Morris, R. E.; Wuttke, S. Toxicity of metalorganic framework nanoparticles: from essential analyses to potential applications. *Chem. Soc. Rev.* **2022**, *51* (2), 464–484.
- (25) Zuidema, J. M.; Kumeria, T.; Kim, D.; Kang, J.; Wang, J.; Hollett, G.; Zhang, X.; Roberts, D. S.; Chan, N.; Dowling, C.; Blanco-Suarez, E.; Allen, N. J.; Tuszynski, M. H.; Sailor, M. J. Oriented Nanofibrous Polymer Scaffolds Containing Protein-Loaded Porous Silicon Generated by Spray Nebulization. *Adv. Mater.* **2018**, *30*, No. 1706785.
- (26) Kim, D.; Zuidema, J. M.; Kang, J.; Pan, Y.; Wu, L.; Warther, D.; Arkles, B.; Sailor, M. J. Facile Surface Modification of Hydroxylated Silicon Nanostructures Using Heterocyclic Silanes. *J. Am. Chem. Soc.* **2016**, *138* (46), 15106–15109.
- (27) Daneshjou, S.; Dabirmanesh, B.; Rahimi, F.; Khajeh, K. Porous silicon nanoparticle as a stabilizing support for chondroitinase. *Int. J. Biol. Macromol.* **2017**, *94*, 852–858.
- (28) Sahare, P.; Ayala, M.; Vazquez-Duhalt, R.; Agrawal, V. Immobilization of peroxidase enzyme onto the porous silicon structure for enhancing its activity and stability. *Nanoscale Res. Lett.* **2014**, *9* (1), 409.
- (29) Sahare, P.; Ayala, M.; Vazquez-Duhalt, R.; Pal, U.; Loni, A.; Canham, L. T.; Osorio, I.; Agarwal, V. Enhancement of Peroxidase Stability Against Oxidative Self-Inactivation by Co-immobilization with a Redox-Active Protein in Mesoporous Silicon and Silica Microparticles. *Nanoscale Res. Lett.* **2016**, *11*, 417.
- (30) Biewenga, L.; Rosier, B.; Merkx, M. Engineering with NanoLuc: a playground for the development of bioluminescent protein switches and sensors. *Biochem. Soc. Trans.* **2020**, *48* (6), 2643–2655.
- (31) Hall, M. P.; Unch, J.; Binkowski, B. F.; Valley, M. P.; Butler, B. L.; Wood, M. G.; Otto, P.; Zimmerman, K.; Vidugiris, G.; Machleidt, T.; Robers, M. B.; Benink, H. A.; Eggers, C. T.; Slater, M. R.; Meisenheimer, P. L.; Klaubert, D. H.; Fan, F.; Encell, L. P.; Wood, K. V. Engineered Luciferase Reporter from a Deep Sea Shrimp Utilizing

- a Novel Imidazopyrazinone Substrate. ACS Chem. Biol. 2012, 7 (11), 1848–1857.
- (32) Wu, C.-C.; Hu, Y.; Miller, M.; Aroian, R. V.; Sailor, M. J. Protection and Delivery of Anthelmintic Protein Cry5B to Nematodes Using Mesoporous Silicon Particles. *ACS Nano* **2015**, *9* (6), 6158–6167.
- (33) Qin, Z.; Joo, J.; Gu, L.; Sailor, M. J. Size Control of Porous Silicon Nanoparticles by Electrochemical Perforation Etching. *Part. Part. Syst. Charact.* **2014**, *31* (2), 252–256.
- (34) Schroeder, M. M.; Wang, Q.; Badieyan, S.; Chen, Z.; Marsh, E. N. G. Effect of Surface Crowding and Surface Hydrophilicity on the Activity, Stability and Molecular Orientation of a Covalently Tethered Enzyme. *Langmuir* **2017**, *33* (28), 7152–7159.
- (35) Saha, B.; Saikia, J.; Das, G. Correlating enzyme density, conformation and activity on nanoparticle surfaces in highly functional bio-nanocomposites. *Analyst* **2015**, *140* (2), 532–542.
- (36) Walker, J. R.; Hall, M. P.; Zimprich, C. A.; Robers, M. B.; Duellman, S. J.; Machleidt, T.; Rodriguez, J.; Zhou, W. Highly Potent Cell-Permeable and Impermeable NanoLuc Luciferase Inhibitors. *ACS Chem. Biol.* **2017**, *12* (4), 1028–1037.
- (37) Hayer-Hartl, M.; Bracher, A.; Hartl, F. U. The GroEL-GroES Chaperonin Machine: A Nano-Cage for Protein Folding. *Trends Biochem. Sci.* **2016**, *41* (1), 62–76.
- (38) Gupta, A. J.; Haldar, S.; Miličić, G.; Hartl, F. U.; Hayer-Hartl, M. Active cage mechanism of chaperonin-assisted protein folding demonstrated at single-molecule level. *J. Mol. Biol.* **2014**, *426* (15), 2739–54.
- (39) Serdakowski, A. L.; Dordick, J. S. Enzyme activation for organic solvents made easy. *Trends Biotechnol.* **2008**, *26* (1), 48–54.
- (40) Porello, I.; Cellesi, F. Intracellular delivery of therapeutic proteins. New advancements and future directions. *Front. Bioeng. Biotechnol.* **2023**, *11*, No. 1211798.